2D transition metal carbide MXene as a robust biosensing platform for enzyme immobilization and ultrasensitive detection of phenol

Lingxia Wu[a,c], Xianbo Lu[a,*], Dhanjai[a], Zhong-Shuai Wu[b], Yanfeng Dong[b], Xiaohui Wang[d], Shuanghao Zheng[b,c], Jiping Chen[a]

[a] CAS Key Laboratory of Separation Science for Analytical Chemistry, Dalian Institute of Chemical Physics, Chinese Academy of Sciences, 457 Zhongshan Road, Dalian 116023, PR China
[b] Dalian National Laboratory for Clean Energy, Dalian Institute of Chemical Physics, Chinese Academy of Sciences, 457 Zhongshan Road, Dalian 116023, PR China
[c] University of Chinese Academy of Sciences, Beijing 100049, PR China
[d] Shenyang National Laboratory for Materials Science, Institute of Metal Research, Chinese Academy of Sciences, Shenyang 110016, PR China

ARTICLE INFO

ABSTRACT

MXene-Ti_3C_2, as a new class of two-dimensional (2D) transition metal carbides (or nitrides), has been synthesized by exfoliating pristine Ti_3AlC_2 phases with hydrofluoric acid. The SEM and XRD images show that the resultant MXene possesses a graphene-like 2D nanostructure. and the surface of MXene has been partially terminated with -OH, thus providing a favorable microenvironment for enzyme immobilization and retaining their bioactivity and stability. Considering the unique metallic conductivity, biocompatibility and good dispersion in aqueous phase, the as-prepared MXene was explored as a new matrix to immobilize tyrosinase (a model enzyme) for fabricating a mediator-free biosensor for ultrasensitive and rapid detection of phenol. The varying electrochemical measurements were used to investigate the electrochemical performance of MXene-based tyrosinase biosensors. The results revealed that the direct electron transfer between tyrosinase and electrode could be easily achieved via a surface-controlled electrochemical process. The fabricated MXene-based tyrosinase biosensors exhibited good analytical performance over a wide linear range from 0.05 to 15.5 μmol L^{-1}, with a low detection limit of 12 nmol L^{-1} and a sensitivity of 414.4 mA M^{-1}. The proposed biosensing approach also demonstrated good repeatability, reproducibility, long-term stability and high recovery for phenol detection in real water samples. With those excellent performances, MXene with graphene-like structure is proved to be a robust and versatile electrochemical biosensing platform for enzyme-based biosensors and biocatalysis, and has wide potential applications in biomedical detection and environmental analysis.

1. Introduction

With the growing interest in low dimensional nanomaterials, two-dimensional (2D) transition metal carbides or nitrides called MXenes have attracted extensive attention due to their unique morphology and properties. The 2D layered MXenes are synthesized by selectively removing "A" layers from bulk $M_{n+1}AX_n$ phases (where M is an early transition metal, A is an A-group mostly from groups 13 and 14 of a periodic table, and X is C and/or N, n = 1–3) (Barsoum, 2000), resulting in the chemical formula of $M_{n+1}X_n$. Because the metallic nature of the M-A bond is weaker than the M-X bond, the etching procedure can be successfully achieved (Meshkian et al., 2015).

Ti_3AlC_2 is one of the 70-plus group of ternary carbides and nitrides ($M_{n+1}AX_n$), and the MXene-Ti_3C_2 can be obtained by exfoliating Ti_3AlC_2 with hydrofluoric acid (Naguib et al., 2011). Due to the

unsaturated surface with unpaired electrons, the surfaces of MXene-Ti_3C_2 are easily terminated with various functional groups (e.g., -O, -OH or/and -F group) during the etching procedure without changing the metallic conductivity (Khazaei et al., 2013; Zhang and Dong, 2017). The formation of strong bonds between the Ti and the attached groups make the surface-functionalized Ti_3C_2 more stable. The mechanical flexibility of O-functionalized Ti_3C_2 improves a lot because of the significant charge transfer from the inner Ti-C bonds to the outer Ti-O surface (Fu et al., 2016; Guo et al., 2015). When the surface of MXene-Ti_3C_2 adsorbs the -OH group, the interlayer coupling in the OH-terminated Ti_3C_2 is stronger than that in the F- or O-terminated one attributing to the formation of hydrogen bonds between the layers in the former (Khazaei et al., 2017). With the intriguing physical and chemical properties, such as graphene-like structure, large electrochemically active surface, metallic conductivity, high stability, excellent

---

* Corresponding author.
  E-mail address: xianbolu@dicp.ac.cn (X. Lu).

mechanical properties, especially good dispersion in aqueous solution (Eames and Islam, 2014; Naguib et al., 2011, 2014), MXene has been widely used in metal (Li, Na, K, Ca) ion batteries (Dong et al., 2017; Er et al., 2014; Mashtalir et al., 2013), supercapacitors (Lukatskaya et al., 2013; Zha et al., 2016; Zhang and Dong, 2017), fuel cells (Xie et al., 2013), absorbents (Mashtalir et al., 2014; Peng et al., 2014), electronic devices (Liu et al., 2015; Lorencova et al., 2017; Rakhi et al., 2016; Wang et al., 2014, 2015).

Enzyme biosensors, as alternative analytical tools, have been extensively used for on-site monitoring environmental pollutants for the advantages of simplified operation, cost-efficient, fast response, inexpensive instrument and minimal requirement for sample pretreatment. The biosensing materials play an important role for the development of enzyme biosensor (Wu et al., 2012a). To date, carbon-based nanomaterials, such as graphene, carbon nanotube and mesoporous carbon, have been widely used as biosensing materials for enzyme immobilization and biosensor fabrication, due to their large specific surface areas, good biocompatibility and excellent electrical conductivity. However, these nanocarbons always have hydrophobic nature, which is difficult to disperse uniformly in water phase. As is well known, the uniform dispersion of nanomaterials in water solution is crucial to advance their applications in enzyme-based biosensors. In order to alter the hydrophobic surface, these nanocarbons were functionalized with hydroxyl or carboxylic groups (Malig et al., 2012; Si and Samulski, 2008; Xu et al., 2008) and amphiphilic polymers or surfactants (Lotya et al., 2009). Although, the solubility of the nanomaterials were improved, it is inevitable to decrease their electrical conductivity and introduce other materials to the biosensing platform. In our previous study, room temperature ionic liquids (RTILs) were used to alter the solubility of graphene (Lu et al., 2014) and mesoporous carbon (Wu et al., 2012b). The hydrophobic nanomaterials become water-soluble and remain the excellent electrical conductivity, but the high-purity RTILs are very expensive and the preparation process of RTIL-carbon nanocomposite is highly complicated yet time-consuming. Therefore, MXene with hydrophylic surface and excellent metallic conductivity could be a good candidate as an excellent immobilization matrix for fabricating electrochemical biosensors. Up to date, MXene-Ti_3C_2 either in pristine form or combined with TiO_2 nanoparticles has been used to immobilize Hemoglobin for the detection of H_2O_2 or $NaNO_2$ (Liu et al., 2015; Wang et al., 2014, 2015), displaying good performances. To the best of our knowledge, the studies about MXenes for enzyme-based biosensors are very limited (Rakhi et al., 2016). Considering the unique structure and excellent properties of MXenes, more systematic studies about MXenes for enzyme immobilization and biosensor fabrication should be carried out.

In this study, MXene-Ti_3C_2 has been synthesized by exfoliating pristine Ti_3AlC_2 phases with hydrofluoric acid. The resultant MXene possesses a graphene-like 2D nanostructure and the conductivity are comparable with those of multilayer graphenes (Naguib et al., 2014). More importantly, the surfaces of MXene have been partially terminated with -OH, which could provide an aqueous-like biocompatible microenvironment for the immobilized enzyme molecules and retaining their bioactivity and stability (Das and Prabhu, 1990; Lu et al., 2006). Considering the unique metallic conductivity, biocompatibility and good dispersion in aqueous phase, the as-prepared MXene-Ti_3C_2 was explored as a matrix to immobilize tyrosinase (Tyr, a model enzyme) for fabricating a mediator-free biosensor. The resulting MXene-Ti_3C_2 based biosensor exhibited excellent analytical performances with high sensitivity, fast response and low detection limit for determination of phenol. The proposed biosensing method also demonstrated good repeatability, reproducibility, long-term stability and high recovery for phenol detection in water samples. The MXene-Ti_3C_2 with graphene-like structure is evidenced to be a robust electrochemical biosensing platform for enzyme-based biosensors, and has wide potential applications in biomedical detection and environmental analysis.

2. Materials and methods

2.1. Materials

Chitosan (Chi, from shrimp shells, $\geq 75\%$ deacetylated) and tyrosinase (from mushroom, $> 1000\,units\,mg^{-1}$) were purchased from Sigma (USA). Phenol was purchased from J&K Chemical Ltd. (Beijing, China). $50\,mmol\,L^{-1}$ phosphate buffer solution (PBS, pH 6.0) were prepared by mixing standard solutions of Na_2HPO_4 and NaH_2PO_4. Unless otherwise stated, PBS ($50\,mmol\,L^{-1}$, pH 6.0) was deoxygenated and used as the electrolyte in electrochemical experiments. Milli-Q water ($18\,M\Omega\,cm$) was used throughout all experiments.

2.2. Apparatus and methods

Scanning electron microscopy (SEM) images were obtained with a field emission scanning electron microscopy JSM-7800F (JEOL, Japan). The powder X-ray diffraction (XRD) patterns were obtained on a X′pert Pro X-ray diffractometer (PANalytical, Holland) with Cu $K_{\alpha 1}$ radiation ($\lambda = 1.5406\,\text{Å}$) over the 2θ range of $5-80°$. The scan step-width was set to $0.033°$ and the scan rate was $0.1°\,s^{-1}$ at room temperature. Fourier transform infrared (FTIR) spectra were obtained by using a Spectrum GX apparatus (Perkin-Elmer Company, USA).

Electrochemical impedance spectroscopy (EIS) measurements were carried out with a Metrohm Autolab PGSTAT 302 N Potentioatat/Galvanostat (Eco Chemie, The Netherlands) in a $1\,mmol\,L^{-1}$ $K_3[Fe(CN)_6]/K_4[Fe(CN)_6]$ (1:1) solution containing $0.5\,mol\,L^{-1}$ KNO_3, with a scan frequency range from 1×10^4 to 1×10^{-1} Hz and an amplitude of 10 mV. Cyclic voltammetry (CV) and current-time (I-t) measurements were carried out on glassy carbon electrodes (GC, 3 mm diameter) by using a CHI 440B electrochemical workstation (CHI Instruments Inc., USA). The measurements were based on a three-electrode system consisting of the modified GC electrode as the working electrode, an Ag/AgCl electrode (KCl concentration of $3\,mol\,L^{-1}$) as the reference electrode, and a platinum wire as the auxiliary electrode.

2.3. Preparation of MXene

Firstly, the pristine Ti_3AlC_2 was prepared by the solid-liquid reaction (Hu et al., 2016). Briefly, the elemental powders of Ti, Al and graphite in a molar ratio of 3: 1.1: 1.88 were mixed with agate balls and then heated to 1550 °C for 2 h in a following argon atmosphere. Then, MXene-Ti_3C_2 was synthesized by exfoliating the pristine Ti_3AlC_2 phases with hydrofluoric acid (HF) (Naguib et al., 2012, 2011). Typically, 1.0 g Ti_3AlC_2 powder was slowly added to 120 mL 40 wt% hydrofluoric acid solution. The reaction mixture was stirred at 300 rpm for 72 h at 25 °C. After that, the mixed solution was centrifuged at 6000 rpm for 5 min, and the powder was collected after discarding the supernatant. Then, the resulting powder was washed with distilled water repeatedly four times. Finally, Ti_3C_2 was collected by filtering the solution using a polytetrafluoroethylene membrane (0.22 mm pore size) and dried in vacuum oven at 60 °C for 12 h.

2.4. Construction of MXene based tyrosinase biosensor

The MXene based tyrosinase biosensor was prepared by a simple casting method. Prior to modification, a GC electrode with 3 mm diameter was polished on a polishing cloth with 1.0, 0.3 and 0.05 μm alumina powder successively, and washed with Milli-Q water followed by sonicating in ethanol and Milli-Q water. Then the electrode was dried with purified nitrogen stream. With the optimization of the experimental conditions, the final compositions containing tyrosinase, MXene, and chitosan were $2.5\,mg\,mL^{-1}$, $0.4\,mg\,mL^{-1}$ and $1.5\,mg\,mL^{-1}$, respectively. The preparation process of biosensor was as follows: Firstly, $10\,\mu L$ tyrosinase solution ($10\,mg\,mL^{-1}$, dissolved in PBS) was added into $20\,\mu L$ MXene suspension ($0.8\,mg\,mL^{-1}$, dispersed

in water), and the mixture solution was shaking for 20 min. Then, 10 μL chitosan solution (6.0 mg mL^{-1}, dissolved in 2% acetic acid aqueous solution and then adjusted to pH 5.0 using 10% NaOH solution) was injected into the above solution. Finally, 5 μL of the above mixture was cast onto the surface of a freshly polished GC electrode. A beaker was covered over the electrode so that water could evaporate slowly and a uniform film electrode (Tyr-MXene-Chi/GC) was formed at room temperature. When not in use, the fabricated electrode was stored at 4 ℃ in a refrigerator. Other enzyme electrodes were prepared by the similar procedures as described above. Before electrochemical measurements, all the as-prepared enzyme electrodes were immersed in 50 mmol L^{-1} PBS (pH 6.0) for 30 min to remove residual components.

2.5. Detection of phenol by Tyr-MXene-Chi/GC biosensor

CV measurements were carried out in pH 6.0 PBS at a scan rate of 100 mV s^{-1} ranging from + 0.4 V to − 0.4 V. The amperometric current-time curves for phenol were carried out to comparatively study the performance of different biosensors. Under an applied potential value of − 0.04 V, the measurements were performed in 8 mL stirring PBS with successive addition of standard phenol solution at appropriate time intervals at room temperature. Real water samples were also detected by similar amperometric current-time curve method.

3. Results and discussion

3.1. SEM and XRD characterization of MXene

In this work, the MXene-Ti$_3$C$_2$ nanosheets were synthesized by exfoliating the Al layer from the pristine Ti$_3$AlC$_2$ phases with HF at room temperature (Naguib et al., 2012, 2011). And the as-prepared MXene-

Ti$_3$C$_2$ nanosheets were characterized by means of SEM and XRD (Fig. 1).

Fig. 1A clearly shows the synthesized MXene-Ti$_3$C$_2$ crystallites exhibit microscale bulk sheets with graphene-like multilayer nanostructure, and the average thickness of the exfoliated multilayers is less than 20 nm, indicating that the MXene has a large specific surface area for tyrosinase to immobilize. The unique 2D graphene-like nanostructure of MXene provides a large surface area for tyrosinase entrapment, and the tyrosinase molecules can be absorbed by surface functional groups of MXene. As shown in Fig. 1B, a compact composite film of Tyr-MXene-Chi was formed on the GC electrode. The 2D nanostructure provided by MXene are favorable for entrapped enzymes to retain their bioactivities and to facilitate the transport of enzymatic substances and products, and the porous structure of composite film (Tyr-MXene-Chi film) improved the effective surface area of the modified electrode, leading to improved performance of fabricated biosensor.

The MXene-Ti$_3$C$_2$ was scanned over the 2θ range of 5−80° to identify the crystal structure. As shown in Fig. 1C, there are several very sharp diffraction peaks, indicating a crystalline state. The major diffraction characteristic peaks have been observed at 8.98°, 18.3°, 27.6°, 34.3°, 43.4° and 60.7°, which are in good agreement with the previously reported XRD spectra of Ti$_3$C$_2$(OH)$_2$ (Naguib et al., 2011), indicating the crystalline material MXene-Ti$_3$C$_2$ with the surface ligand of -OH has been achieved. During the etching procedure, the unsaturated surface with unpaired electrons of as-prepared MXene-Ti$_3$C$_2$ could be easily terminated with various functional groups (-O, -F, and/or -OH) (Khazaei et al., 2013). Because the preparation of MXene was carried out in an aqueous environment with rich -OH, the surface of MXene-Ti$_3$C$_2$ was partially terminated with -OH functional group (Wang et al., 2014). As is well known, the dispersibility of nanomaterials in aqueous
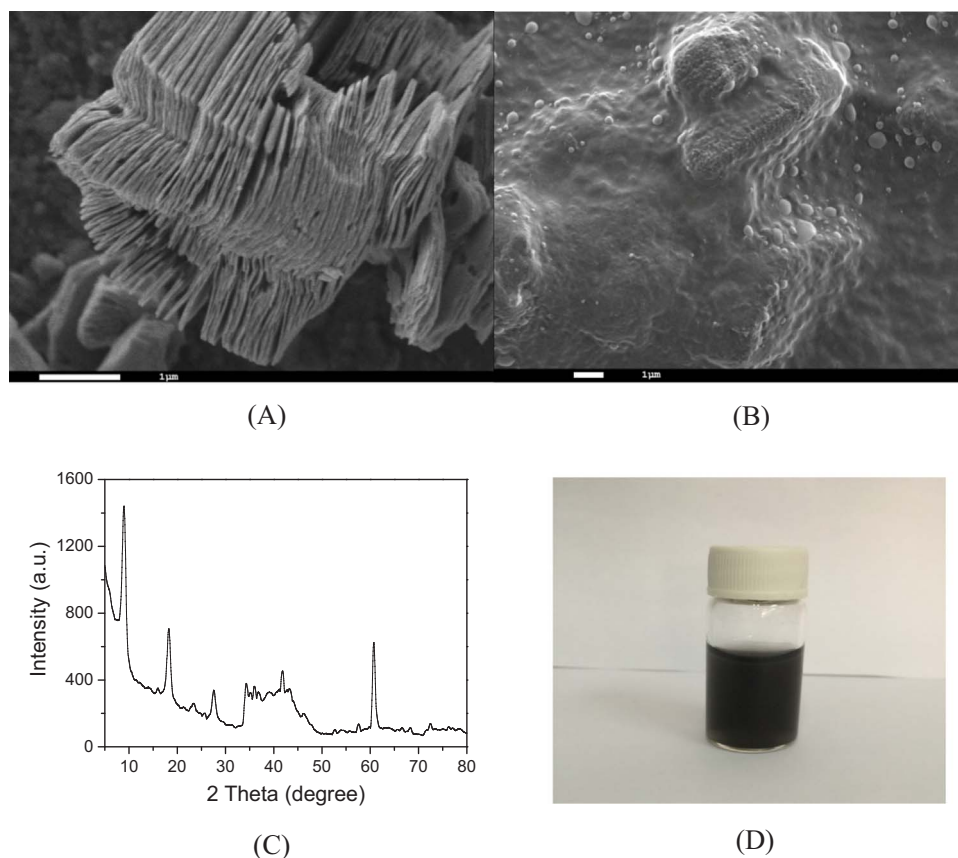

(A)   (B)

(C)   (D)

Fig. 1. (A) Typical SEM images of MXene. (B) SEM images of Tyr-MXene-Chi film on electrode. (C) XRD image of MXene. (D) Photograph of 0.8 mg mL^{-1} MXene-Ti$_3$C$_2$ dispersion in aqueous solution.
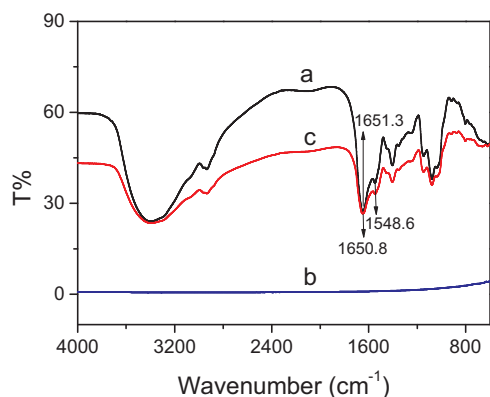
Fig. 2. FT-IR spectra of Tyr (a), MXene (b), andTyr-MXene (c).

solution plays a key role for their application in biosensors, bioelectronics, etc. Due to the abundant surface hydroxyl group, the as-prepared MXene could disperse uniformly in aqueous phase (Fig. 1D), which brings great convenience and also many advantages (e.g. improved stability and reproducibility of biosensors) for its application in enzyme-based biosensors.

3.2. FT-IR characterization of tyrosinase, MXene and tyrosinase-MXene nanocomposite

FT-IR is a most effective means to study the secondary structure of tyrosinase intercalated into the MXene nanosheets. And the vibrational bands of the amide I and amide II are used to identify the secondary structure of tyrosinase. The amide I band (1700–1600 cm^{-1}) is corresponding to the -C꞊O stretching vibration of peptide linkages in backbone of protein. The amide II band (1620–1500 cm^{-1}) is attributed to the combination of -N-H bending and C-N stretching (Lu et al., 2008). As shown in Fig. 2b, MXene-Ti$_3$C$_2$ has no absorption peaks from 4000 to 600 cm^{-1}. Fig. 2a shows the characteristic peaks of tyrosinase appear at 1548.6 cm^{-1} and 1651.3 cm^{-1}. The absorption peaks of Tyr-MXene nanocomposite (Fig. 2c) appear at 1548.6 cm^{-1} and 1650.8 cm^{-1}, which are similar to the characteristic absorption peaks of native tyrosinase, suggesting the tyrosinase molecules retain its native secondary structure after forming Tyr-MXene hierachical nanocomposites, and revealing the good biocompatibility of MXene-Ti$_3$C$_2$. The slight shift of amide I band (from 1651.3 to 1650.8 cm^{-1}) indicates there might be some interaction between tyrosinase and MXene-Ti$_3$C$_2$ matrix. The interaction might be caused by electrostatic interaction and hydrogen bond interaction between the tyrosinase and OH-terminated MXene-Ti$_3$C$_2$. The aqueous-like biocompatible microenvironment provided by the hydrophilic surfaces of OH-terminated MXene-Ti$_3$C$_2$ are beneficial for stabilizing the immobilized tyrosinase (Das and Prabhu, 1990). The MXene-Ti$_3$C$_2$ based nanocomposite film may provide a favorable microenvironment for tyrosinase immobilization because of its good biocompatibility and multilayer nanostructure.

3.3. CV and EIS characterization of MXene modified electrodes

The CV responses of different modified electrodes in 1 mM Fe(CN)$_6^{3-/4-}$ solution containing 0.1 M KCl were demonstrated in Fig. 3A. A pair of redox peaks were obtained at bare GC electrode (curve a). However, the presence of Tyr-Chi film significantly diminished the reduction/oxidation peak current of Fe(CN)$_6^{3-/4-}$ on the GC electrode (curve c). Clearly, after MXene nanosheets were doped into Tyr-Chi film, the corresponding electrochemical response of Tyr-MXene-Chi/GC was increased significantly (curve b). This increased cyclic voltammetric response should be ascribed to the high surface area and excellent metallic conductivity of MXene.

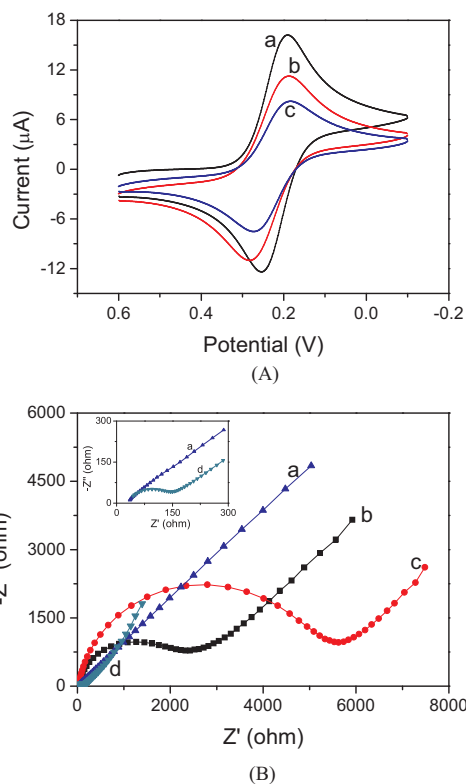EIS is another powerful technique to characterize the interface

Fig. 3. (A) CVs of bare GC (a), Tyr-MXene-Chi/GC (b), Tyr-Chi/GC (c) in 1 mM Fe(CN)$_6^{3-/4-}$ solution containing 0.1 M KCl. Scan rate: 100 mV s^{-1}. (B) Nyquist plots of bare GC (a), Tyr-MXene-Chi/GC (b), Tyr-Chi/GC (c), Chi/GC (d) in 1 mmol L^{-1} K$_3$[Fe(CN)$_6$]/K$_4$[Fe(CN)$_6$] (1:1) containing 0.5 mol L^{-1} KNO$_3$. Insert: Amplified Nyquist plot of (a) bare/GC and (d) Chi/GC.

properties of nanocomposite film modified GC electrodes. Fig. 3B shows the impedance spectrum of bare GC, Chi/GC, Tyr-Chi/GC, and Tyr-MXene-Chi/GC in 1 mmol L^{-1} K$_3$[Fe(CN)$_6$]/K$_4$[Fe(CN)$_6$] (1:1) solution containing 0.5 mol L^{-1} KNO$_3$. In the Nyquist plot, there is a semicircular part and a linear part. The semicircular part at high frequencies corresponds to the electron transfer process and its diameter is equal to the electron transfer resistance (Rct). The linear part at lower frequencies corresponds to the diffusion process (Feng et al., 2005; Sagara et al., 1990). As shown in Fig. 3B, Nyquist plot of bare GC electrode was nearly a straight line, indicating that it was almost a diffusion limiting process and the electron transfer rate between bare GC electrode and [Fe(CN)$_6$]$^{3-/4-}$ was the fastest. When the electrode surface was modified by specific composite, the value of Rct changed because of the steric hindrance and electrostatic interactions (Bonanni et al., 2012). The Rct of chitosan modified GC electrode (99 Ω) was larger than that of bare GC electrode, indicating that the layer of chitosan had formed on the electrode which hinder the electron transfer between the redox probe of [Fe(CV)$_6$]$^{3-/4-}$ and the electrode surface. Though the chitosan could hinder the electron transfer, it is a good linear polymer with excellent film-forming ability for constructing electrochemical biosensors (Wu et al., 2012a). After the tyrosinase was combined with chitosan to modify GC electrode, the Rct increased from 99 Ω to 4.74 kΩ indicating the tyrosinase had been successfully immobilized on the electrode. As demonstrated in Fig. 3b and Fig. 3c, with MXene further immobilized on the Tyr-Chi film, the Rct significantly decreased from 4.74 kΩ to 2.01 kΩ. The improved interfacial conductivity could be ascribed to the introduction of MXene, which acted as nanoscale electrodes and promoted the electron transfer of [Fe(CN)$_6^{3-/4-}$] to the surface of electrode.

3.4. CV and amperometric characterization of MXene based biosensor

To evaluate the bioelectrochemical activity of Tyr-MXene-Chi/GC,
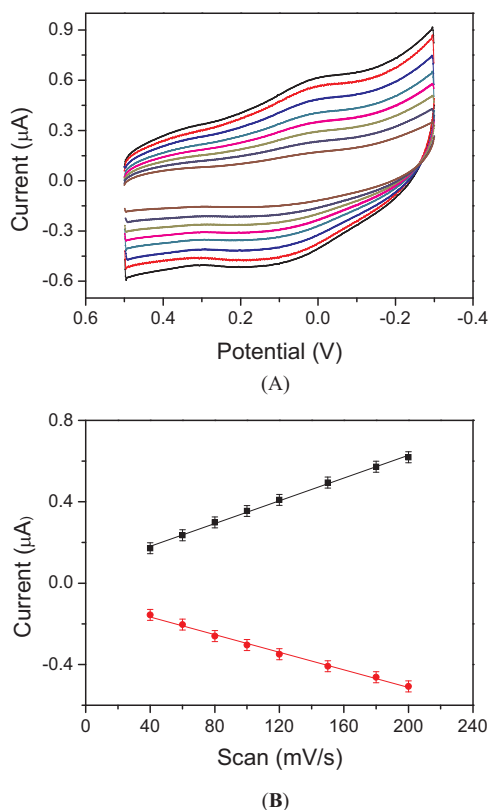
(A)

(B)

Fig. 4. (A) CV curves of Tyr-MXene-Chi/GC in pH 6.0 PBS with different scan rates (from inner to outer: 40, 60, 80, 100, 120, 150, 180, 200). (B) Calibration plot of cathodic and anodic peak currents vs. scan rates.

the fabricated electrodes were characterized by CV in the presence of phenol at the potential range from + 0.4 to − 0.4 V. Fig. 4A shows the typical CV of the Tyr-MXene-Chi/GC in nitrogen-saturated PBS (50 mmol L^{-1}, pH 6.0) at various scan rates. As shown in Fig. 4B, the cathodic and anodic peak currents increased linearly with the increasing scan rates. This indicated that the electron transfer between tyrosinase and GC electrode could be easily performed at the Tyr-MXene-Chi composite film and it was a surface-controlled electrochemical process. According to Laviron's equation (Laviron, 1974), for a surface-controlled process, the peak currents are directly proportional to the scan rates, thus the peak currents increase with the increased scan rates accordingly. In addition, both the cathodic and anodic peak potentials are independent of the scan rates. According to the Laviron method for a surface-controlled electrochemical system (Laviron, 1979), the apparent heterogeneous electron transfer rate constant (k_s) of tyrosinase immobilized on Tyr-MXene-Chi/GC was estimated to be about 1.62 s^{-1}, which was higher than that 0.66 s^{-1} for tyrosinase immobilized on graphene choline-gold electrode (He et al., 2017) and 1.15 ± 0.04 s^{-1} for Tyr/NiO nanoparticles modified GC electrode (Moghaddam et al., 2008), suggesting a faster electron-transfer process.

The detection mechanism of phenol based on electrochemical tyrosinase biosensor has been described in previous study (Wu et al., 2012b). Firstly, in the presence of oxygen, the phenol could be oxidized into the corresponding o-quinone by tyrosinase biosensor. And then, the obtained o-quinone could be electrochemically reduced to the corresponding polyhydric phenol on the electrode surface to cyclically amplify the electrochemical signal of phenol. Based on the above mechanism, the electrochemical tyrosinase biosensor is a powerful tool for the rapid detection of phenolic pollutants. Fig. 5 shows the CV of the Tyr-MXene-Chi/GC in the absence of phenol (curve a) and in the presence of 3 μmol L^{-1} phenol (curve b) in air-saturated PBS (50 mmol L^{-1}, pH 6.0) at a scan rate of 100 mV s^{-1}. After injecting

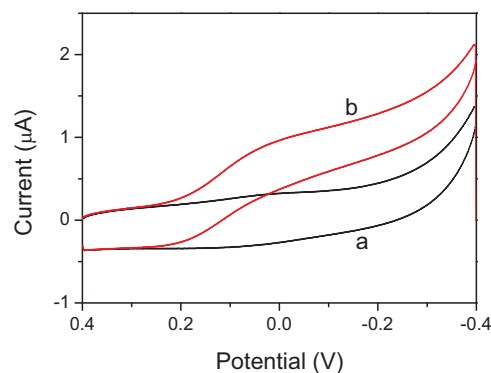**Fig. 5.** CVs of the Tyr-MXene-Chi/GC biosensor in the absence of phenol (a) and in the presence of 3 μmol L^{-1} phenol (b) in air-saturated 50 mM pH 6.0 PBS at a scan rate of 100 mV s^{-1}.

3 μmol L^{-1} phenol, both the oxidation current and reduction current increased obviously. The increase of redox currents indicated that the enzyme-catalyzed reaction occurred on the electrode surface and the tyrosinase immobilized on the electrode remained highly biocatalytic activity for phenol. As shown in Fig. 5, a large response toward phenol was observed at a relatively low potential of − 0.04 V. In order to effectively reduce the possible background and have a lower detection limit, the relative low potential (− 0.04 V versus Ag/AgCl) was selected as the constant working potential for further amperometric study.

Compared to CV method, amperometry is a more sensitive electrochemical method for phenol detection. Fig. 6A illustrates and compares the amperometric I-t curves of Tyr-MXene-Chi/GC (curve a), Tyr-
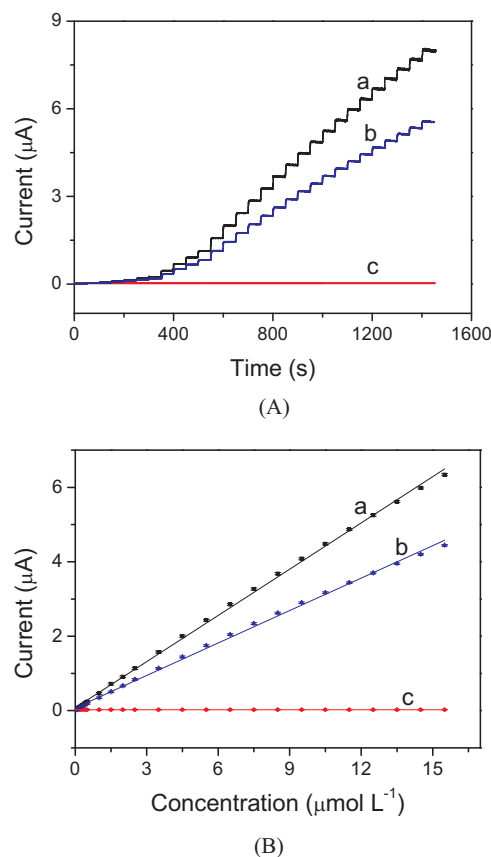

(A)

(B)

Fig. 6. (A) Amperometric current-time response curves of Tyr-MXene-Chi (a), Tyr-Chi (b) and MXene-Chi (c) with successive additions of phenol with different concentrations into a stirring 50 mM PBS (pH 6.0, 8 mL). Applied potential: − 0.04 V versus Ag/AgCl. (B) The corresponding calibration curves of steady-state currents versus concentrations of phenol.

Chi/GC (curve b), MXene-Chi/GC (curve c) at -0.04 V with the successive additions of phenol to 50 mmol L^{-1} PBS under constant stirring. The MXene-Chi/GC without tyrosinase completely had no response to the changing concentration of phenol (Fig. 6A, curve c). However, well-defined amperometric signals were observed for the electrodes modified with Tyr-Chi and Tyr-MXene-Chi with the addition of phenol, indicating the tyrosinase remained its biocatalytic activity after immobilizing on the electrode. The response time of Tyr-MXene-Chi/GC is less than 5 s (achieving 96% of steady state current). Such a rapid response of Tyr-MXene-Chi biosensor could be attributed to the fast diffusion of phenol from the external solution into the tyrosinase molecules immobilized on MXene nanosheets and its fast bioelectrocatalytic reaction. Fig. 6B shows the typical calibration curves of the response currents of these biosensors versus the concentrations of phenol. As shown in Fig. 6B, the steady-state response currents increased with the increasing concentrations of phenol. The sensitivity of Tyr-MXene-Chi/GC is 414.4 mA M^{-1}, which was about 1.5 times than that of Tyr-Chi/GC (290.8 mA M^{-1}). The linear range of the MXene based biosensor was ranging from 5.0×10^{-8} to 15.5×10^{-6} mol L^{-1} with a correlation coefficient of 0.999. As a biosensor, the limit of detection (LOD) is one of the most important performances. The LOD of Tyr-MXene-Chi/GC biosensor was estimated to be 12 nmol L^{-1} at a signal-to-noise ratio of 3, which was better than that of mesoporous carbon modified tyrosinase electrode (20 nmol L^{-1}) (Wu et al., 2012b) and graphene-Au-Chi-Tyr modified screen-printed carbon electrode (16 nM) (Fartas et al., 2017).

The good biosensing performance with lower LOD and a wider linear range of the Tyr-MXene-Chi/GC biosensor could be attributed to the following aspects: firstly, the graphene-like structure of MXene with large specific surface area could enlarge the active surface area of the GC electrode available for enzyme immobilization, which increased the surface loading quantity of enzyme. Meanwhile, the MXene-enzyme hybrid structure provided a favorable microenvironment for the enzyme to retain its activity and stability. The MXene-based biosensor can be a promising and robust electrochemical biosensing platform for ultrasensitive and rapid detection of phenol.

3.5. Reproducibility, stability and real sample application of the biosensor

The repeatability, reproducibility and stability of the Tyr-MXene-Chi/GC biosensors were evaluated by amperometry for the detection of 0.5 μM phenol. A relative standard deviation (RSD) value of intraelectrode was 1.6%, which was obtained for 7 successive determinations, indicative of good repeatability of this method. Similarly, the electrode-to-electrode fabrication reproducibility was evaluated by three electrodes prepared under the same conditions. The RSD of these three individual biosensors was 1.3%, revealing excellent electrode-to-electrode reproducibility. The enzyme electrodes were sealed and stored in a refrigerator at 4 °C when not in use. The storage stability of the biosensor was evaluated by the CV response to 1.5 μM phenol. The results showed that the biosensor retained 89% of the original response after 6 weeks, revealing good long-term stability.

In order to further evaluate the performance of Tyr-MXene-Chi/GC biosensor for real sample analysis, the recovery test was studied by adding spiked phenol into tap water. The tap water samples were filtered through 0.45 μm filter membrane before use in order to remove suspended solids. The samples were evaluated by amperometry for determining the response of tap water spiked with 0.5 μM phenol, and the recovery was from 86.8% to 106% (see Table S1 in the Supplementary information) for three tested electrodes. The results reveal that the as-fabricated biosensor is a reliable tool for the rapid and efficient detection of phenol in real water samples.

4. Conclusions

In summary, 2D MXene-Ti_3C_2 nanosheets was prepared by exfoliating pristine Ti_3AlC_2 with HF. The MXene-Ti_3C_2 possesses unique metallic conductivity, biocompatibility and good dispersion in aqueous phase. Based on graphene-like MXene-Ti_3C_2, a mediator-free biosensing platform was successfully fabricated by a facile way for ultrasensitive and rapid detection of phenol. Benefiting from the large specific area, excellent electronic conductivity, biocompatibility and good dispersion in aqueous phase, the fabricated tyrosinase biosensor exhibited good sensitivity, repeatability and stability, with a low detection limit and a wide linear range. The Tyr-MXene-Chi/GC biosensor was further used for rapid detection of phenol in tap water with a satisfactory result. The mediator-free biosensor based on MXene-Ti_3C_2 provides a simple, sensitive, rapid and cost-effective method for the detection of phenol in water samples. The MXene-Ti_3C_2 proves to be a promising candidate for enzyme immobilization and may have wide potential applications in biomedical detection and environmental analyses.

Acknowledgements

Appendix A. Supplementary material

Supplementary data associated with this article can be found in the online version at http://dx.doi.org/10.1016/j.bios.2018.02.021.

References

Barsoum, M.W., 2000. Prog. Solid State Chem. 28 (1), 201–281.
Bonanni, A., Loo, A.H., Pumera, M., 2012. TrAC Trends Anal. Chem. 37, 12–21.
Das, G., Prabhu, K.A., 1990. Enzym. Microb. Technol. 12 (8), 625–630.
Dong, Y., Wu, Z.S., Zheng, S., Wang, X., Qin, J., Wang, S., Shi, X., Bao, X., 2017. ACS Nano 11 (5), 4792–4800.
Eames, C., Islam, M.S., 2014. J. Am. Chem. Soc. 136 (46), 16270–16276.
Er, D., Li, J., Naguib, M., Gogotsi, Y., Shenoy, V.B., 2014. ACS Appl. Mater. Interfaces 6 (14), 11173–11179.
Fartas, F.M., Abdullah, J., Yusof, N.A., Sulaiman, Y., Saiman, M.I., 2017. Sensors 17 (5), 1132.
Feng, J.J., Zhao, G., Xu, J.J., Chen, H.Y., 2005. Anal. Biochem. 342 (2), 280–286.
Fu, Z.H., Zhang, Q.F., Legut, D., Si, C., Germann, T.C., Lookman, T., Du, S.Y., Francisco, J.S., Zhang, R.F., 2016. Phys. Rev. B 94 (10), 104103.
Guo, Z., Zhou, J., Si, C., Sun, Z., 2015. Phys. Chem. Chem. Phys.: PCCP 17 (23), 15348–15354.
He, Y., Yang, X., Han, Q., Zheng, J., 2017. Molecules 22 (7), 1047.
Hu, M., Li, Z., Hu, T., Zhu, S., Zhang, C., Wang, X., 2016. ACS Nano 10 (12), 11344–11350.
Khazaei, M., Arai, M., Sasaki, T., Chung, C.-Y., Venkataramanan, N.S., Estili, M., Sakka, Y., Kawazoe, Y., 2013. Adv. Funct. Mater. 23 (17), 2185–2192.
Khazaei, M., Ranjbar, A., Arai, M., Sasaki, T., Yunoki, S., 2017. J. Mater. Chem. C 5 (10), 2488–2503.
Laviron, E., 1974. J. Electroanal. Chem. Interfacial Electrochem. 52 (3), 355–393.
Laviron, E., 1979. J. Electroanal. Chem. Interfacial Electrochem. 101 (1), 19–28.
Liu, H., Duan, C., Yang, C., Shen, W., Wang, F., Zhu, Z., 2015. Sens. Actuators B: Chem. 218, 60–66.
Lorencova, L., Bertok, T., Dosekova, E., Holazova, A., Paprckova, D., Vikartovska, A., Sasinkova, V., Filip, J., Kasak, P., Jerigova, M., Velic, D., Mahmoud, K.A., Tkac, J., 2017. Electrochim. Acta 235, 471–479.
Lotya, M., Hernandez, Y., King, P.J., Smith, R.J., Nicolosi, V., Karlsson, L.S., Blighe, F.M., De, S., Wang, Z., McGovern, I.T., Duesberg, G.S., Coleman, J.N., 2009. J. Am. Chem. Soc. 131, 3611–3620.
Lu, X., Wen, Z., Li, J., 2006. Biomaterials 27 (33), 5740–5747.
Lu, X., Zhou, J., Lu, W., Liu, Q., Li, J., 2008. Biosens. Bioelectron. 23 (8), 1236–1243.
Lu, X., Wang, X., Jin, J., Zhang, Q., Chen, J., 2014. Biosens. Bioelectron. 62, 134–139.
Lukatskaya, M.R., Mashtalir, O., Ren, C.E., Dall'Agnese, Y., Rozier, P., Taberna, P.L., Naguib, M., Simon, P., Barsoum, M.W., Gogotsi, Y., 2013. Science 341 (6153), 1502–1505.
Malig, J., Romero-Nieto, C., Jux, N., Guldi, D.M., 2012. Adv. Mater. 24 (6), 800–805.
Mashtalir, O., Naguib, M., Mochalin, V.N., Dall'Agnese, Y., Heon, M., Barsoum, M.W., Gogotsi, Y., 2013. Nat. Commun. 4, 1716.
Mashtalir, O., Cook, K.M., Mochalin, V.N., Crowe, M., Barsoum, M.W., Gogotsi, Y., 2014. J. Mater. Chem. A 2 (35), 14334–14338.
Meshkian, R., Näslund, L.-Å., Halim, J., Lu, J., Barsoum, M.W., Rosen, J., 2015. Scr. Mater. 108, 147–150.

Moghaddam, B.A., Ganjali, M.R., Saboury, A.A., Moosavi-Movahedi, A.A., Norouzi, P., 2008. J. Appl. Electrochem. 38 (9), 1233–1239.

Naguib, M., Kurtoglu, M., Presser, V., Lu, J., Niu, J., Heon, M., Hultman, L., Gogotsi, Y., Barsoum, M.W., 2011. Adv. Mater. 23 (37), 4248–4253.

Naguib, M., Mashtalir, O., Carle, J., Presser, V., Lu, J., Hultman, L., Gogotsi, Y., Barsoum, M.W., 2012. ACS Nano 6 (2), 1322–1331.

Naguib, M., Mochalin, V.N., Barsoum, M.W., Gogotsi, Y., 2014. Adv. Mater. 26 (7), 992–1005.

Peng, Q., Guo, J., Zhang, Q., Xiang, J., Liu, B., Zhou, A., Liu, R., Tian, Y., 2014. J. Am. Chem. Soc. 136 (11), 4113–4116.

Rakhi, R.B., Nayuk, P., Xia, C., Alshareef, H.N., 2016. Sci. Rep. 6, 36422.

Sagara, T., Niwa, K., Sone, A., Hinnen, C., Niki, K., 1990. Langmuir: ACS J. Surf. Colloids 6 (1), 254–262.

Si, Y., Samulski, E.T., 2008. Nano Lett. 8 (6), 1679–1682.

Wang, F., Yang, C., Duan, C., Xiao, D., Tang, Y., Zhu, J., 2014. J. Electrochem. Soc. 162 (1), B16–B21.

Wang, F., Yang, C., Duan, M., Tang, Y., Zhu, J., 2015. Biosens. Bioelectron. 74, 1022–1028.

Wu, L., Deng, D., Jin, J., Lu, X., Chen, J., 2012a. Biosens. Bioelectron. 35 (1), 193–199.

Wu, L., Lu, X., Zhang, H., Chen, J., 2012b. ChemSusChem 5 (10), 1918–1925.

Xie, X., Chen, S., Ding, W., Nie, Y., Wei, Z., 2013. Chem. Commun. 49 (86), 10112–10114.

Xu, Y., Bai, H., Lu, G., Li, Ch, Shi, G., 2008. J. Am. Chem. Soc. 130, 5856–5857.

Zha, X.-H., Yin, J., Zhou, Y., Huang, Q., Luo, K., Lang, J., Francisco, J.S., He, J., Du, S., 2016. J. Phys. Chem. C 120 (28), 15082–15088.

Zhang, J.J., Dong, S., 2017. J. Chem. Phys. 146 (3), 034705.